Materials & Design 247 (2024) 113375

Contents lists available at ScienceDirect

Materials & Design

journal homepage: www.elsevier.com/locate/matdes

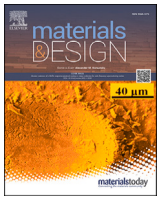

Utilizing polydispersity in three-dimensional random fibrous based sound absorbing materials

Quang Vu Tran [a,b,c,*], Camille Perrot [a,*], Raymond Panneton [b,*], Minh Tan Hoang [c], Ludovic Dejaeger [c], Valérie Marcel [c], Mathieu Jouve [c]

[a] Univ Gustave Eiffel, Univ Paris Est Creteil, CNRS, UMR 8208, MSME, F-77454, Marne-la-Vallée, France
[b] Département de Génie Mécanique, Université de Sherbrooke, J1K 2R1, Québec, Canada
[c] Adler Pelzer Group, Acoustic TechCenter R&D, Z.I. François Sommer – BP13, 08210, Mouzon, France

ARTICLE INFO

Keywords:
Multiscale model
Fibrous materials
Polydispersity
Transport properties
Sound absorption
Optimization

ABSTRACT

The distribution of fiber diameters plays a crucial role in the transport and sound absorbing properties of a three-dimensional random fibrous (3D-RF) medium. Conventionally, volume-weighted averaging of fiber diameters has been utilized as an appropriate microstructural descriptor to predict the static viscous permeability of 3D-RF media. However, the long wavelength acoustical properties of a 3D-RF medium are also sensitive to the smallest fibers, this is particularly true in the high-frequency regime. In our recent research, we demonstrated that an inverse volume-weighted averaging of fiber diameters can effectively serve as a complementary microstructural descriptor to capture the high-frequency behavior of polydisperse fibrous media. In the present work, we reexamine the identification of two representative volume elements (RVEs) which relies on the reconstruction of 3D-RF microstructures having volume-weighted and inverse-volume weighted averaged fiber diameters, respectively in the low-frequency and high frequency regimes. We investigate the implication of such a weighting procedure on the transport and sound absorbing properties of polydisperse fibrous media, highlighting their potential advantages. Furthermore, we discuss the challenges associated with this research field. Finally, we provide a brief perspective of the future directions and opportunities for advancing this area of study.

1. Introduction

Three-dimensional random fibrous (3D-RF) structures have become one of the most widespread technologies in large-scale manufacturing of sound-absorbing materials known as nonwovens or felts, employing various types of fibers to achieve their acoustical constraints. Some commonly used manufacturing processes include the airlay process [1,2] and the carding, cross-lapping, and needing process [3,4]. Traditional thermobonded airlaid nonwoven typically incorporates a mixture of non-homogeneous shoddy fibers (75%) and bicomponent fibers (25%) in the airlay process. The bicomponent fibers have a core made from PET and a surface made from coPET. On the other hand, to facilitate recycling, needlefelt nonwoven use a mixture of PET fibers (60%) and bicomponent fibers (40%). In both cases, in post-processing, the nonwoven materials are reinforced by thermobonding (with a chosen compression ratio), where the bicomponent fibers have an adhesive effect. However, the use of non-homogeneous fibers in the manufacturing process comes with some drawbacks.

One of the disadvantages is that the transport mechanisms can be significantly impacted by the fiber size variations induced by the manufacturing process. For example, shoddy fibers are obtained after the tearing of textile waste from a mixture of 55% cotton and 45% PET, and cotton fibers can introduce fiber dust particles, which affect the distribution of fiber diameters. The manufacturing process of nonwoven leads to a wide distribution of fiber diameters and fiber orientations, which affects the frequency-dependent response of the fluid within the corresponding 3D-RF structure. Moreover, mixing fibers of different sizes is generally recommended. The largest fibers ensure the rigidity and mechanical stability of the nonwoven material, while the smallest fibers provide sound absorbing capabilities to the fibrous materials.

Therefore, an important research direction in this field is the study of various distributions of fiber diameters and orientations and the

* Corresponding authors.
E-mail addresses: quang.vu.tran@usherbrooke.ca (Q.V. Tran), camille.perrot@univ-eiffel.fr (C. Perrot), raymond.panneton@usherbrooke.ca (R. Panneton).

https://doi.org/10.1016/j.matdes.2024.113375
Received 16 August 2024; Received in revised form 8 October 2024; Accepted 13 October 2024
Available online 17 October 2024

development of models that account for the corresponding frequency-dependent response functions. Several approaches have been explored to achieve this goal. Perhaps the most direct method is to conduct a series of laboratory measurements on samples of varying fiber size and orientation (semi-empirical models) [5–7]. Alternatively, in the quest for theoretical understanding, one may seek to better understand the mathematical (analytical derivations) [8–13] or physical (semi-phenomenological description) [14–17] basis of the generalized (dynamic) Darcy-scaled equations for macroscopic transport. Lastly, one can consider studies based on numerical simulations [18–20]. Notably, Peyrega and Jeulin [21] used a volume-weighted average diameter $D_v = \sum_{i=1}^{N_f} V_i D_i / \sum_{i=1}^{N_f} V_i$ to successfully predict the static viscous permeability of heterogeneous fibrous materials and our group [22] has recently demonstrated that an inverse volume weighted average diameter $D_{iv} = \sum_{i=1}^{N_f} \frac{D_i}{V_i} / \sum_{i=1}^{N_f} \frac{1}{V_i}$ can serve as a complementary microstructural descriptor to predict the characteristic lengths and tortuosity of these polydisperse 3D random fibrous materials. In the previous definitions, V_i represents the volume of fiber i with diameter D_i and N_f the number of fibers introduced in the RVE. The non-weighted average diameter is given by $D_m = \frac{1}{N_f} \sum_{i=1}^{N_f} D_i$.

In this paper, we aim to provide a comprehensive report of research advancements in employing 3D polydisperse RF microstructures, with a particular emphasis on using polydispersity as a new lever of optimization [23–25]. Starting from existing specimens of nonwoven fibrous materials, we focus specifically on three different types of studies: (i) a parametric study, using the coefficient of variation CV defined as the ratio of the standard deviation to the mean of the fiber diameters and used to express the polydispersity degree P_d of random fibrous media as input parameter; (ii) optimizing the sound absorption average at normal incidence over a wide frequency range of a given nonwoven specimen by controlling the degree of polydispersity of the fiber diameters; (iii) achieving targets of industrial interest consisting of lowering the lower frequency from which the sound absorption in a diffuse field is greater than 80%. The paper is organized in the following sequences. In the first section, we delve into the fundamental transport properties of 3D-RF microstructures used as sound-absorbing materials that are characterized by a wide distribution of their fiber diameters. We discuss the unique transport properties and microstructural descriptors derived from the polydispersity of these materials, highlighting their potential advantages over traditional fibrous materials. This section serves as a foundation for understanding the subsequent discussions. Building upon the understanding of 3D microstructure based RF materials, we dedicate the second section to exploring the advantages offered by employing specific polydispersity degree as a microstructural optimization lever. We discuss the benefits associated with tuning the polydispersity degree of 3D-RF microstructures in terms of their transport properties, sound absorption average at normal incidence, sound absorption targets in diffuse field. By doing so, we highlight our contribution to the field, showing the advancements that could be achieved by leveraging the polydisperse feature of the these materials to enhance their functional properties. Finally, we conclude the article with a brief perspective and outlook on current challenges and the future of research in this area. We discuss emerging challenges, potential directions for further explorations, and the significance of continued investigations into 3D-RF microstructured materials as a microstructural optimization lever of their physical properties. By summarizing the current state of the field and presenting potential avenues for future research, we aim to inspire and guide researchers in this exciting area of study.

2. Nonwoven fibrous media characterized by local heterogeneity

2.1. Predicting transport properties

Martys and Garboczi [19] demonstrated through numerical computations the important effect spatial randomness in the pore space has on flow problems. In particular, they established a crucial distinction between the electric fields and the fluid-flow fields for a given pore structure. Leveraging this distinction, they identified that in a random pore structure with a distribution of pore sizes, the fluid-flow will tend to go more through the largest pore necks; while the electrical current-flow rate was comparatively more sensitive to the width of narrow necks. As a result, the fluid velocity fields and the electric fields can sample the pore space quite differently. Subsequently, Peyrega and Jeulin [21] made substantial advances in this area, particularly in identifying the volume-weighted average diameter (D_v in our notations) as a key microstructural descriptor for the determination of the representative volume element (RVE) of a random fibrous medium. Moreover, Tran [22] and collaborators delved into the associated microscopic basis of macroscopic viscous permeability, shedding further light on how macroscopic viscous permeability depends on the largest pore sizes of a locally heterogeneous 3D-RF microstructure. The volume-weighed average diameter D_v of a wide distribution of fiber diameters is larger than non-weighted average diameter D_m, and the number of introduced fibers in a cubic box of normalized size L/D_m is therefore lower in the volume-weighted average diameter case (D_v) than in the non-weighted average diameter one (D_m) – while the porosity ϕ is known and given by measurements in both cases. As a result, the reconstructed pore sizes of 3D-RF structures having a volume-weighted average diameter D_v match with the largest pore necks through which the viscous fluid-flow will tend to go in the corresponding nonwoven specimen. This reconstruction procedure enables the identification of a RVE having D_v as the average diameter and the computed viscous permeability k_0 to be consistent with the measured values [$L/D_m = 25(-)$, $L = 400\ \mu m$] in real samples whose sample diameters [$S_D = 45\ mm$], are much larger than those of the RVE [22].

The combined presence of a wide distribution of fiber diameters and random microstructure promotes pore-size local heterogeneity, leading to the identification of the volume-weighted average diameter D_v, as being an appropriate microstructural descriptor for the prediction of the static viscous permeability k_0. The use of the finite element method revealed that velocity fields are consistent with experimental measurements of viscous permeability using volume-weighted average diameter D_v, as shown in Figs. 1(a), 1(d) and 1(j). However, the electric current paths are clearly less concentrated and tortuous than do the fluid-flow paths, so there are significantly fewer stagnant areas for the electrical current flow than for the fluid flow. The viscous characteristic length Λ is defined [26] by the following ratio of integrals: $\Lambda = 2 \int |\mathbf{E}(\mathbf{r})|^2 dV_p / \int |\mathbf{E}(\mathbf{r})|^2 dS$, where $\mathbf{E}(\mathbf{r})$ is the magnitude of the electrical field in the pore space, dV_p is the volume element in the pore space, and dS is the surface element on the pore solid interface. Therefore, Λ can be thought of as a dynamically weighted hydraulic radius [14], where the weighting procedure substantially favors the smaller pores because of current conservation. Fig. 1(c) shows a 3D-RF microstructure where inverse volume-weighted average diameter D_{iv} is used as the appropriate microstructural descriptor for the prediction of the viscous characteristic length Λ. The geometrical reconstruction method is given in a previous work [22]. The smaller pores of the nonwoven polydisperse fibrous materials were probed by measuring the experimental value of the Λ parameter, a value captured by using inverse volume-weighted average diameter D_{iv} during the reconstruction procedure, as shown in Figs. 1(i) and 1(k). The change in pore size reconstruction induced by fiber diameter polydispersity and volume-based fiber diameter weighting is shown in Fig. 1(a)-1(c). At the scale of the reconstructed unit-cell, the non-weighted average diameter D_m was neither an appropriate microstructural descriptor for describing the largest pores connected with viscous fluid flow nor a correct one to identify the smallest dynamically connected pore sizes probed by electrical current flow; Fig. 1(b), 1(e) and 1(h). D_v based and D_{iv} based RVEs predictions all showed excellent agreement respectively with static viscous permeability k_0 and viscous characteristic length Λ measurements over a large range of porosities ϕ; Fig. 1(j) and 1(k).

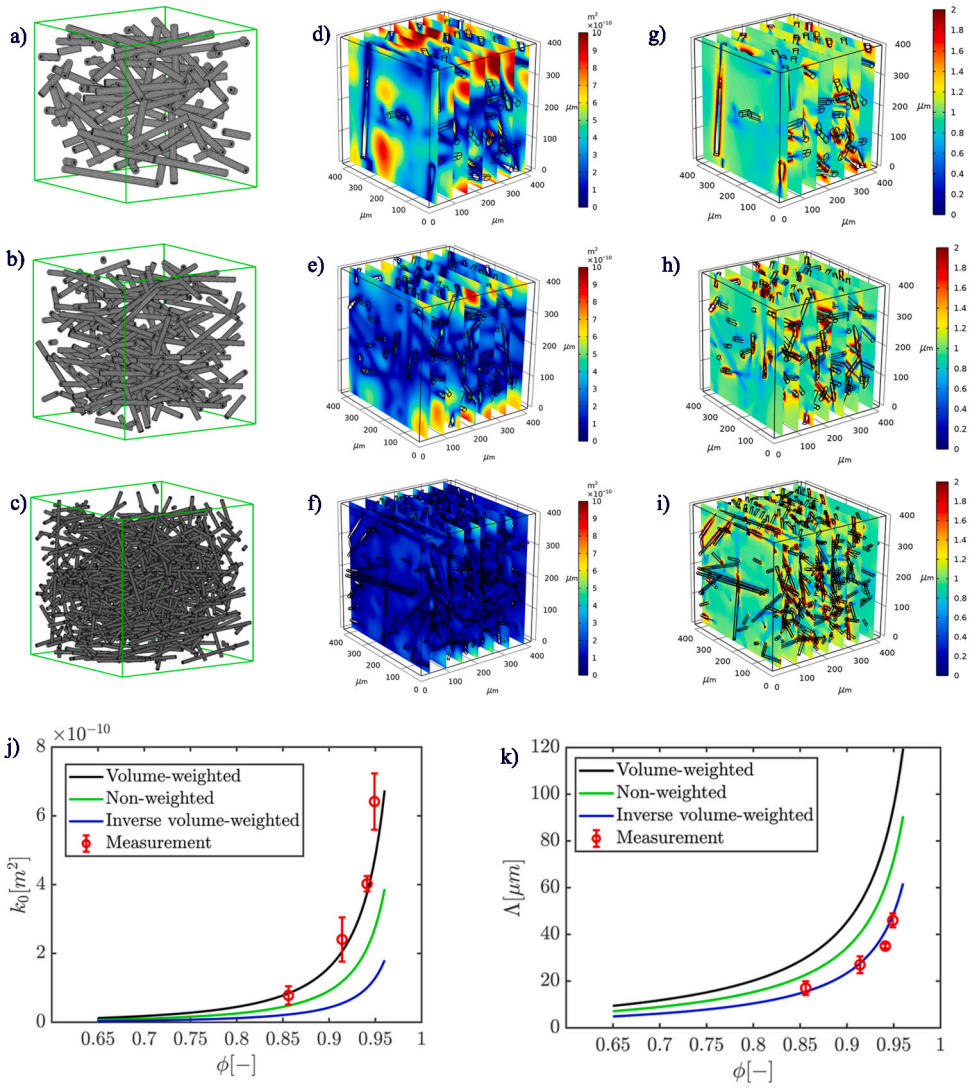

Fig. 1. Effect of polydispersity on the transport properties. (a)-(c) Three-dimensional random fibrous microstructures corresponding to the sample denoted F2 using volume-weighted, non-weighted, inverse volume-weighted average diameters, respectively. (d)-(f) Velocity fields expressed as local permeability ($k_{0zz}[m^2]$) corresponding to Stokes flow in the z direction with the RVE reconstructed using (a) volume weighted, (b) non-weighted and (c) inverse volume-weighted average diameter. (g)-(i) Scaled potential field ($\varphi[m]$ corresponding to potential flow in the z direction [-] with the RVE reconstructed using (a) volume weighted, (b) non-weighted and (c) inverse volume-weighted average diameter. (j) The static viscous permeability $k_0(m^2)$ of nonwoven fibrous materials (F1, F2, F3, F4) as a function of porosity ϕ(-). (k) The viscous characteristic length $\Lambda(\mu m)$ of nonwoven fibrous materials (F1, F2, F3, F4) as a function of porosity ϕ(-).

2.2. Polydispersity effect on the transport properties of three-dimensional random fibrous microstructures

Polydispersity effect occurs when particles of varied sizes in the dispersed phase modifies the expected behavior of the corresponding system. The wide distribution of fiber diameters changes the transport parameters of a 3D-RF microstructure characterized by a sharply peaked distribution of fiber diameters, resulting is a non-conventional RVE. Previous works describe the Gamma-based distribution of fiber diameter configuration and confirm this effect in glass wool, cotton felts and PET felts' composites. [27,22] Fig. 2(a) illustrates the probability density function (PDF) of the Gamma distribution (Γ) of fiber diameters according to the equation

$$f(D;a,b) = \frac{1}{\Gamma(a)b^a} D^{a-1} e^{-\frac{D}{b}}, \tag{1}$$

where D is the fiber diameter of the probability distribution function parameterized with the shape a ($a > 0$) and scale b ($b > 0$) parameters. Fig. 2(b) shows the geometry of 3D-RF structures with an increasing coefficient of variation $CV = 1/\sqrt{a}$ used as a measure of dispersion; at $CV = 20\%$, $CV = 50\%$, and $CV = 100\%$. The corresponding porosity is equal to $\phi = 94.1\%$ and the mean fiber diameter is given by $D_m = ab = 14\mu m$. The RVEs based on D_v and based on D_{iv} are presented in Fig. 2(c) and 2(d), respectively. Coefficient of variation was around 40% in the cotton felts case (F1-F4) and 30% in the PET felts one, and the orientation of fibers of the 3D-RF microstructures was parameterized assuming transverse isotropy according to an additionally needed factor, the angular orientation parameter Ω_{zz} ($0 \leq \Omega_{zz} \leq 1$) [28,29]. Therefore, assuming a Gamma-based distribution of fiber diameters, geometrical parameters of the model include porosity ϕ, mean fiber diameter D_m, coefficient of variation of the fiber diameters CV and angular orientation of fibers Ω_{zz}. There exist a strong analogy between the visco-inertial frequency-dependent response function of a Newtonian fluid-filled rigid porous medium [14], and its frequency-dependent thermal counterpart [30,15]. Therefore, the D_v-based cell was simultaneously utilized as the RVE to compute the static viscous permeability k_0 and the static thermal permeability k_0'. On the other hand, on the asymptotic high frequency range, the D_{iv}-based cell was used as the RVE for the calculation of the viscous Λ and thermal Λ' characteristic lengths together with the tor-

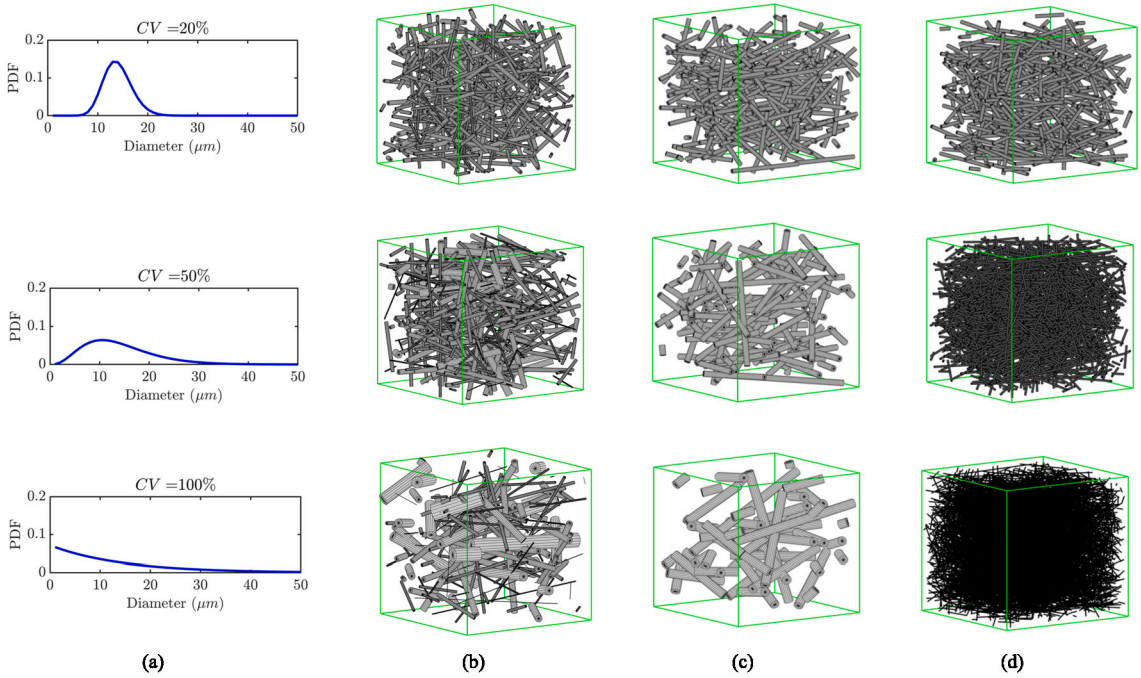

Fig. 2. Polydispersity effect on the representative elementary volumes of three-dimensional random fibrous microstructures. (a) The probability distribution function of Gamma-based fiber diameters ($D_m = 14\mu m$) for increasing coefficients of variation CV of fiber diameters ($CV = 20\%$, $CV = 50\%$, $CV = 100\%$). (b) Geometric reconstruction of corresponding three-dimensional random fibrous microstructures ($\phi = 94.1\%$). Geometric reconstructions of (c) D_v-based and (d) D_{iv}-based representative elementary volumes used to predict the viscous fluid flow and electrical current flow effective transport properties of polydisperse fibrous media.

tuosity α_∞. The fiber diameters' dispersion effects for the D_v-based cell and D_{iv}-based cell is shown in Fig. 3. Fig. 3 demonstrates a significant increase of the volume-weighted average diameter, D_v, with respect to the corresponding mean diameter D_m, for an increasing coefficient of variation CV of the Gamma-based law. This increase of D_v/D_m can be characterized by a polynominal function of second order with respect to CV. Meanwhile, the inverse volume-weighted diameter D_{iv} undergoes an exponential decrease as the coefficient of variation CV of the fiber diameters increases, due to the increasing amount of small fibers present in the probability distribution function for high levels of CV (Fig. 2a). This indicates that polydisperse 3D-RF microstructures having D_v and D_{iv} based cells as RVEs can introduce drastic contrasts in the local characteristic sizes (D_v; D_{iv}) and the corresponding asymptotic transport parameters (k_0, k_0'; Λ, Λ', α_∞) owing to their strong and different sensitivities to the extreme values of the distribution. These findings suggest that the polydisperse-based RF microstructures effectively exhibit a tuning effect for the design of sound absorbing fibrous materials.

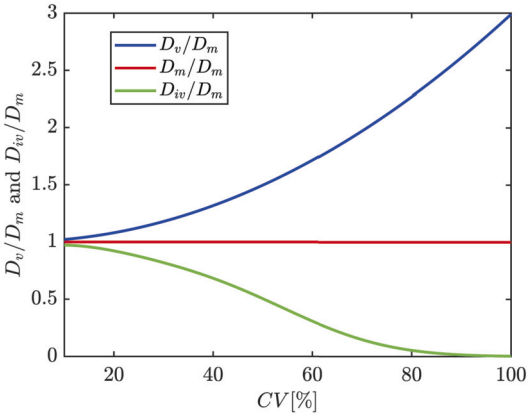

Fig. 3. Evolution of the volume-weighted average diameter D_v and the inverse volume-weighted average diameter D_{iv} as a function of the polydispersity degree P_d of a fiber diameters' distribution quantified through the coefficient of variation CV of a Gamma-based law at constant mean diameter D_m.

2.3. Advantages

Replacing the monodisperse fiber diameters with polydisperse 3D materials can significantly enhance the viscous k_0 and thermal k_0' static permeabilities. It can also reduce the viscous Λ and thermal Λ' characteristic lengths, increase the sound absorption average (SAA), and enhance the diffuse field sound absorption coefficient (SAC_{DF}).

2.3.1. Tuning transport parameters

In this study, we analyze the evolution of transport properties as a function of the coefficient of variation CV for two different families of composite microstructures: composite felts (F1-F4) and PET felts (B1-B2). Fig. 4 illustrates the transport parameters of these 3D-RF microstructures when increasing the coefficient of variation CV of the fiber diameters (at unchanged porosities ϕ and orientation of fibers Ω_{zz}). We observe a quadratic increase in the dimensionless static viscous k_0/r_m^2 and thermal k_0'/r_m^2 permeabilities (with $r_m = D_m/2$), while the dimensionless viscous Λ/r_m and thermal Λ/r_m characteristic lengths show an exponential decrease with CV, and both the ratio Λ'/Λ and the tortuosity α_∞ remain independent of the polydispersity (α_∞ is independent of the length scale of the microstructure). This suggests that controlling the polydispersity of fiber diameters through the coefficient of variation CV with the manufacturing process provides a new lever for optimizing sound-absorbing fibrous materials. The following two sections present examples of CV optimization to respectively improve the sound absorption average and the diffuse field sound absorption based on the optimization algorithm detailed in Appendix A.

2.3.2. Increasing sound absorption average

The sound absorption average at normal incidence (SAA_{NI}) of a material is computed with its sound absorption coefficients at normal

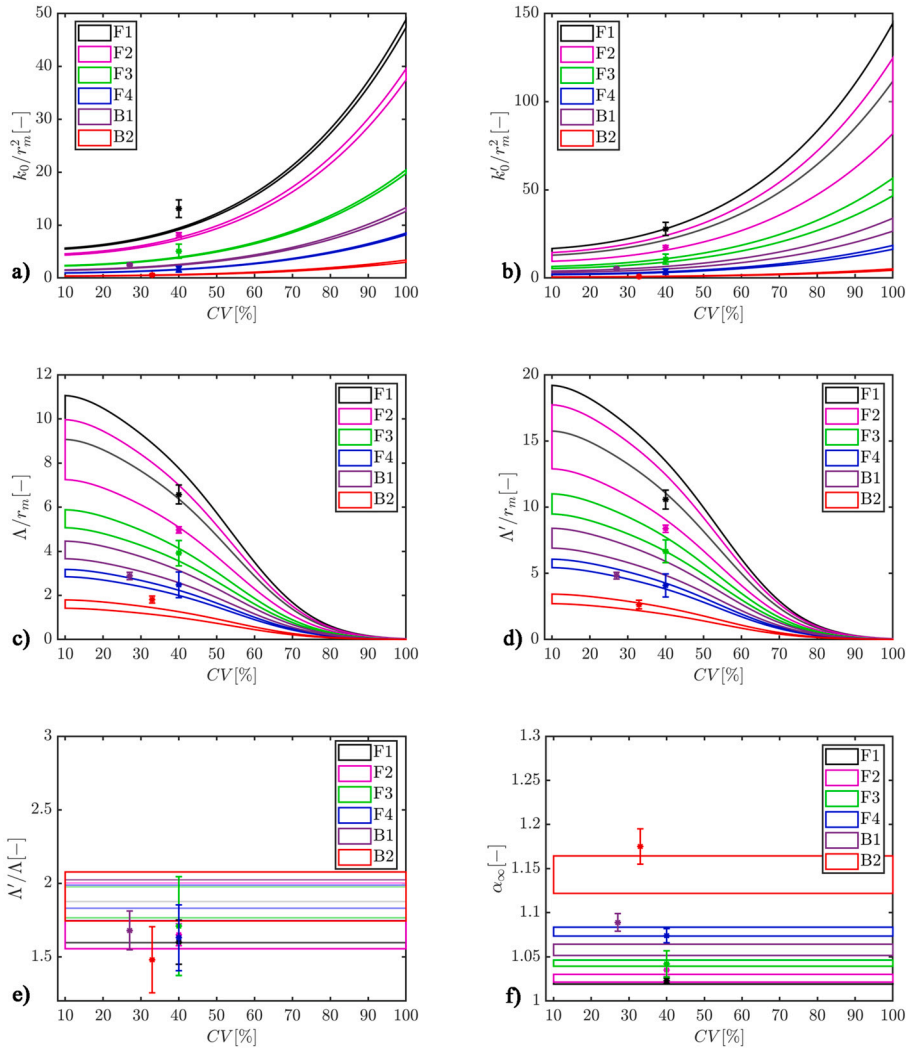

Fig. 4. Dimensionless transport parameters as a function of the coefficient of variation CV of fiber diameters for cotton felts (F1-F4) and PET felts (B1-B2). The porosities ϕ and orientation of fibers Ω_{zz} of each felt are unchanged with CV and taken from measurement. [22] The dots correspond to the experimentally determined values of CV in the initial state of polydispersity and are reported along with the corresponding error bars used to indicate the uncertainty determined in the experimental characterization with available samples. The envelope in the model originates from the uncertainty in the porosity determination.

incidence (SAC_{NI}) at 16 one-third octave bands f_i from 125 to 4500 Hz with

$$SAA_{NI}^{125-4000} = \frac{1}{16}\sum_{f_i=125}^{4500} SAC_{NI}(f_i), \tag{2}$$

Here, the SAC_{NI} is calculated with the material of thickness L_s placed on a hard reflecting backing. Consequently, SAA_{NI} is a measure of the energy dissipated by visco-thermal losses in the material for a unit incident acoustic power. This single number rating is an important coefficient that can be used for characterizing the sound absorbing properties of porous materials in a large frequency range, including low frequencies. We have previously shown that using polydispersity can significantly modify the transport properties of 3D-RF microstructures at constant porosity ϕ and angular orientation Ω_{zz} (Sec. 2.3.1). Fig. 5 shows how the sound absorption average at normal incidence $SAA_{NI}^{125-4000}$ can be maximized by optimization of the CV from the initial set of studied materials (F1-F4; B1-B2). The increase in $SAA_{NI}^{125-4000}$ in 3D-RF microstructures is due to a larger fiber diameter polydispersity ($CV \simeq 75\%$) that allows for a strong contrast between the largest fibers that dominate transport phenomena in the low frequency regime (k_0; k_0') and the smallest fibers that govern transport phenomena in the high frequency regime (Λ, α_∞; Λ'); see Table 1. The results show that the optimized 3D-RF materials (controlled by polydispersity) exhibit lower viscous f_v and thermal f_t transition frequencies than the initial materials – which allowed visco-thermal dissipation mechanisms to occur in a lower frequency range. Another striking result emerging from these simulations is to find that $M = 8k_0\alpha_\infty/\Lambda^2\phi \gg 1$ in the polydisperse cases. We recall that we used the volume-weighted fiber diameter D_v to compute the low-frequency transport parameters of the polydisperse microstructure, and the inverse volume-weighted fiber diameter D_{iv} to obtain the high-frequency ones. It follows that the dimensionless shape factor M introduced by Johnson et al. [14] is evaluated by combining transport parameters corresponding to different moments of the weighted fiber diameters distribution, and thus to different microstructural features of the same complex microgeometry. This approach suggests that a polydisperse 3D-RF medium is a heterogeneous material where coexist at a mesoscale fibers with different and contrasted characteristic sizes. Then the viscous transport will take place mostly along the "subnetwork" formed by the wider pores, while the electrical or inertial transport at high-frequencies will take place over the entire heterogeneous porous structure due to the absence of viscosity in the electric case, and will be able to probe the narrowest pores.

In the previous calculations, the sound absorbing coefficient at normal incidence, SAC_{NI}, derives from the knowledge of the intrinsic transport parameters of the 3D-RF materials (k_0, k_0', Λ, Λ', α_∞). The

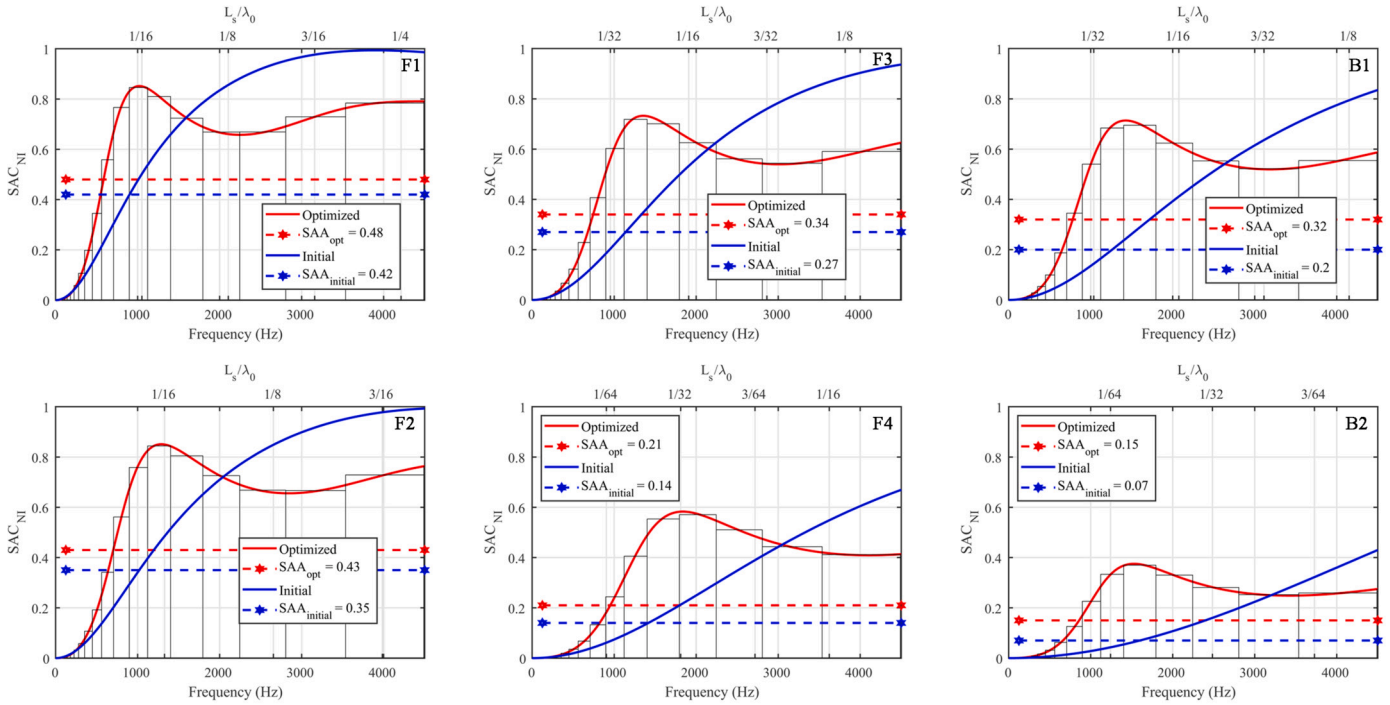

Fig. 5. The sound absorption coefficient at normal incidence, SAA_{NI}, as a function of frequency for the two families of felts studied in this work: Cotton felts (F1-F4) and PET felts (B1-B2). The SAA_{NI} responses obtained prior to modification of the polydispersity (coefficient of variation CV) are shown with a blue line. The red line represents the SAA_{NI} obtained after optimization of the polydispersity by maximizing the SAA_{NI} between the third octave bands from 125 to 4500 Hz. The two dotted lines correspond to the associated single number ratings before (blue) and after (red) optimization.

frequency-dependent response functions, $\tilde{\rho}_{eq}(\omega)$ and $\tilde{K}_{eq}(\omega)$ are described as [14,30,15]

$$\tilde{\rho}_{eq}(\omega) = \frac{\alpha_\infty \rho_0}{\phi}\left[1 + \frac{\phi\eta}{i\omega k_0 \alpha_\infty \rho_0}\sqrt{1 + i\frac{4\alpha_\infty^2 k_0^2 \rho_0 \omega}{\eta \Lambda^2 \phi^2}}\right], \tag{3}$$

and

$$\tilde{K}_{eq}(\omega) = \frac{\gamma P_0/\phi}{\gamma - (\gamma-1)\left[1 - i\frac{\phi\kappa}{k_0'^2 C_p \rho_0 \omega}\sqrt{1 + i\frac{4k_0'^2 C_p \rho_0 \omega}{\kappa \Lambda'^2 \phi^2}}\right]^{-1}}, \tag{4}$$

where $\tilde{\rho}_{eq}(\omega)$ is the equivalent dynamic density, $\tilde{K}_{eq}(\omega)$ is the equivalent bulk modulus, $\omega = 2\pi f$ is the angular frequency, i is the imaginary unit, ρ_0 is the mass density of air, η is the dynamic viscosity of air, P_0 is the atmosphere pressure, $\gamma = C_p/C_v$ is the ratio of heat capacities at constant pressure and volume, and κ is the heat conductivity of air.

By knowing the visco-inertial $\tilde{\rho}_{eq}(\omega)$ and thermal $\tilde{K}_{eq}(\omega)$ response functions of the equivalent fluid of the porous medium, one can determine the wave number $\tilde{q}_{eq}(\omega)$ and the characteristic impedance $\tilde{Z}_{eq}(\omega)$ of the material,

$$\tilde{q}_{eq}(\omega) = \omega\sqrt{\tilde{\rho}_{eq}(\omega)/\tilde{K}_{eq}(\omega)}, \tag{5}$$

$$\tilde{Z}_{eq}(\omega) = \sqrt{\tilde{\rho}_{eq}(\omega)\tilde{K}_{eq}(\omega)}. \tag{6}$$

At normal incidence, the surface impedance $\tilde{Z}_s(\omega)$ and sound absorption coefficient $SAC_{NI}(\omega)$ of a porous material of thickness L_s, backed by a rigid and impervious wall, for any angular frequency ω, are provided by

$$\tilde{Z}_s(\omega) = -i\tilde{Z}_{eq}\cot(\tilde{q}_{eq}L_s), \tag{7}$$

$$SAC_{NI} = 1 - \left|\frac{\tilde{Z}_s - Z_0}{\tilde{Z}_s + Z_0}\right|^2, \tag{8}$$

where $Z_0 = \rho_0 c_0$ is the impedance of the air and c_0 is the sound speed in air.

In Fig. 5, it can be observed that there is a significant change in the wavelength-to-thickness ratio λ_0/L_s, where $\lambda_0 = \omega_0/c_0$, and ω_0 denotes the angular frequency at the first peak absorption. In fact, optimized polydispersed-based 3D-RF microstructures show ratios L_s/λ_0 that can achieve values lower than 1/32 (F4 and B2) - note that the typical ratio for conventional porous materials is around 1/4 (for low resistive material, for which the sound speed is close to that observed in air). This result can be seen as the signature of a certain class of metamaterials called subwavelength material (or slow-sound material). [31] In fact, the optimized properties increase $\tilde{\rho}_{eq}$ and decrease $\tilde{K}_{eq}$. Consequently, the sound speed in the equivalent medium is reduced. These results demonstrate that the use of controlled fiber diameter polydispersity, such as that provided with a gamma distribution shape and characterized with a $CV \sim 80\%$, has the potential to enhance the performance of sound-absorbing nonwoven materials.

2.3.3. Enhancing diffuse field sound absorption

Sound absorbing targets present in the industry for a porous material generally corresponds to a diffuse field (DF) acoustical excitation, satisfying $SAA_{DF} \geq 0.8$, for $f_i \geq f_t$, where f_t is a given one-third octave band. Lowering f_t can lead to various issues in designing sound absorbing materials, as absorbing low frequencies is a challenge that suggests targets of increasing difficulty: $f_t = 1600Hz$ (Target 1), $f_t = 1250Hz$ (Target 2), $f_t = 1000Hz$ (Target 3), $f_t = 800Hz$ (Target 4) and $f_t = 630Hz$ (Target 5). These targets are defined without air gap behind the materials (hard-backed configuration), and the recommended or targeted thickness and mass are usually not mentioned, suggesting that the targets need to be reached with the lowest weight and cost. The sound absorption coefficient in diffuse field, SAC_{DF}, is described as:

Table 1
Transport parameters evolution (ϕ, k_0, k_0', Λ, Λ', α_∞) before (Init.) and after (Opt.) optimization of polydispersity (CV) in the three-dimensional random fibrous microstructures of cotton felts (F1-F4) and PET felts (B1-B2). f_v and f_t represent the visco-inertial and thermal transition frequencies which have been significantly reduced after optimization, which consists in maximizing the sound absorption average at normal incidence across the 16 one-third octave bands (f_i) ranging from 125 to 4500 Hz, $SAA_{NI}^{125-4000}$ [relative increase: F1(14%), F2(23%), F3(26%), F4(50%), B1(60%), B2(114%)].

		CV (%)	ϕ (−)	k_0 ($\times 10^{-10} m^2$)	k_0' ($\times 10^{-10} m^2$)	α_∞ (−)	Λ (μm)	Λ' (μm)	f_v (Hz)	f_t (Hz)	M (−)	$SAA_{NI}^{125-4500}$ (%)
F1	Init.	40.3	0.948	4.5	12.1	1.022	48	84	4668	2557	1.7	42
	Opt.	73.3	0.948	11.1	27.8	1.022	6.9	12	2018	1112	201	48
F2	Init.	39.8	0.941	3.9	9.9	1.026	42	74	5684	3103	1.9	35
	Opt.	74.6	0.941	10.0	27.1	1.026	5.3	9.4	2213	1209	311	43
F3	Init.	41.9	0.914	2.1	5.1	1.042	25	47	10102	5850	3.1	27
	Opt.	72.1	0.914	4.7	13.1	1.042	3.3	6.1	4533	2631	394	34
F4	Init.	38.9	0.856	0.7	1.6	1.077	15	28	25286	17463	3.1	14
	Opt.	73.8	0.856	1.9	5.1	1.077	1.3	2.4	9998	7073	1132	21
B1	Init.	26.6	0.888	2.7	6.3	1.056	42	79	7215	4601	1.5	20
	Opt.	75.5	0.888	9.6	23.1	1.056	3.3	6.1	2116	1356	839	32
B2	Init.	33.1	0.76	0.7	1.2	1.144	15	29	21495	21023	3.7	7
	Opt.	77.6	0.76	2.4	4.3	1.144	0.8	1.6	6690	6518	4516	15

$$SAC_{DF} = \frac{\int_{\theta_{min}}^{\theta_{max}} SAC(\omega,\theta)\cos\theta\sin\theta d\theta}{\int_{\theta_{min}}^{\theta_{max}} \cos\theta\sin\theta d\theta}, \tag{9}$$

where $\theta_{min} = 0^o$ and $\theta_{max} = 90^o$ are the selected diffuse field integration limits.

$SAC(\omega,\theta) = 1 - \left|\frac{\tilde{Z}_s(\omega,\theta)\cos\theta - Z_0}{\tilde{Z}_s(\omega,\theta)\cos\theta + Z_0}\right|^2$ is the sound absorption coefficient at oblique incidence, $\tilde{Z}_s(\omega,\theta) = -i\tilde{Z}_{eq}(\tilde{q}_{eq}/\tilde{q}_x)\cot(\tilde{q}_{eq}L_s)$ is the surface impedance at oblique incidence with $\tilde{q}_x = \sqrt{\tilde{q}_{eq}^2 - q_t^2}$ the longitudinal wave number and $q_t = q_0\sin\theta$ the transverse wave number.

Our simulations suggest that 3D-RF materials, specifically polydisperse with controlled $CV \sim 75\% - 79\%$ can serve as effective sound-absorbing materials in diffuse field to achieve the required industrial targets. By simulating the SAC_{DF} from the initial felts (F1-F4; B1-B2), we identified the optimal coefficient of variation CV allowing to reach the targets of increasing level of difficulty with the minimal thickness. The results, shown in Fig. 6a for the case of cotton felt F1, revealed that none of the targets can be reached from the initial microstructure ($CV = 40.3\%$) and the thickness of the sample ($L_s = 20$ mm). Fig. 6b demonstrated an achievement of Target 1 by using a CV of 78% with a significant reduction of the sample thickness ($L_s = 11$ mm). We obtained similar polydispersity results for the other targets of increasing difficulty (Target 2, $CV = 79\%$, Fig. 6c; Target 3, $CV = 78\%$, Fig. 6d; Target 4, $CV = 77\%$, Fig. 6e; Target 5, $CV = 75\%$, Fig. 6f). However, the sample thicknesses had to be increased (Target 2, $L_s = 13$ mm, Fig. 6c; Target 3, $L_s = 16$ mm, Fig. 6d; Target 4, $L_s = 20$ mm, Fig. 6e; Target 5 $L_s = 27$ mm, Fig. 6f. To better appreciate the performance that has been obtained by increasing and controlling the degree of polydispersity P_d through the coefficient of variation CV of the Gamma law, the results can be plotted in terms of the wavelength-to-thickness ratio, λ_0/L_s. Using a controlled degree of polydispersity allowed us to reach a so-called sub-wavelength sound absorption in the diffuse field, by lowering the maximum sound absorption peak below the quarter-wavelength resonance frequency ($L_s/\lambda_0 = \frac{1}{4}$), indicating a greater ability to absorb low-frequency sound. Therefore, using 3D-RF materials with controlled polydispersity to efficiently absorb low-frequency sound is an important approach as it *a priori* does not require substantial modifications of the manufacturing processes.

3. Outlook and perspective

In this section, we briefly discuss the challenges of this research area and a possible roadmap for a future work.

3.1. Challenges from the manufacturing process

3D-RF microstructures, including cotton felts and PET felts, are commonly manufactured by techniques coming from the textile industry. After their selection, the recycled (shoddy, PET) or noble (bicomponent) fibers are provided within different fineness specified by the $dtex$ unit which enables a linear density estimates of fiber size, such that a corresponding fiber diameter can be determined. However, the model we developed from which we evidenced a strong potential of optimization is not without drawbacks, as it relies on continuous distribution of fiber diameters. Fig. 7 provides the distribution of fiber diameters obtained through SEM images that corresponds to the F1 cotton felt sample and compares this distribution with the one required to reach Target 4 ($CV = 77\%$, same sample thickness). On the left side of the distribution, the fibrous material presents a relatively high number of very thin fibers. The same is also true for the right side of the distribution, where the fibrous material presents a significant amount of large fibers which were merely absent in the initial sample ($2r_f > 30\mu m$). The asymmetry of the probability distribution function suggests a mix of at least six initial families of fibers of different linear densities ($dtex$) with lower CV (15%) to achieve the required distribution. However, the fiber distribution of the corresponding manufactured material may exhibit mismatch compared to the targeted Gamma law. This mismatch is not necessarily problematic if, as expected, the microstructural descriptors governing the physics of the transport parameters are D_v and D_{iv}. Also, the experimental validation of the model is still incomplete, since it relies on samples already manufactured which do not correspond to the expected optimal behavior ($CV \sim 30\% \neq CV \sim 77\%$).

3.2. Future roadmap

In order to address the challenges associated with manufacturing and validation of the model in highly polydispersed 3D-RF microstructures, a crucial aspect of our future roadmap involves the development of a manufacturing method that enables the precise and controlled elaboration of a targeted distribution of polydisperse fiber diameters with $CV \sim 77\%$ from a chosen reduced set of fiber families with $CV \sim 15\%$.

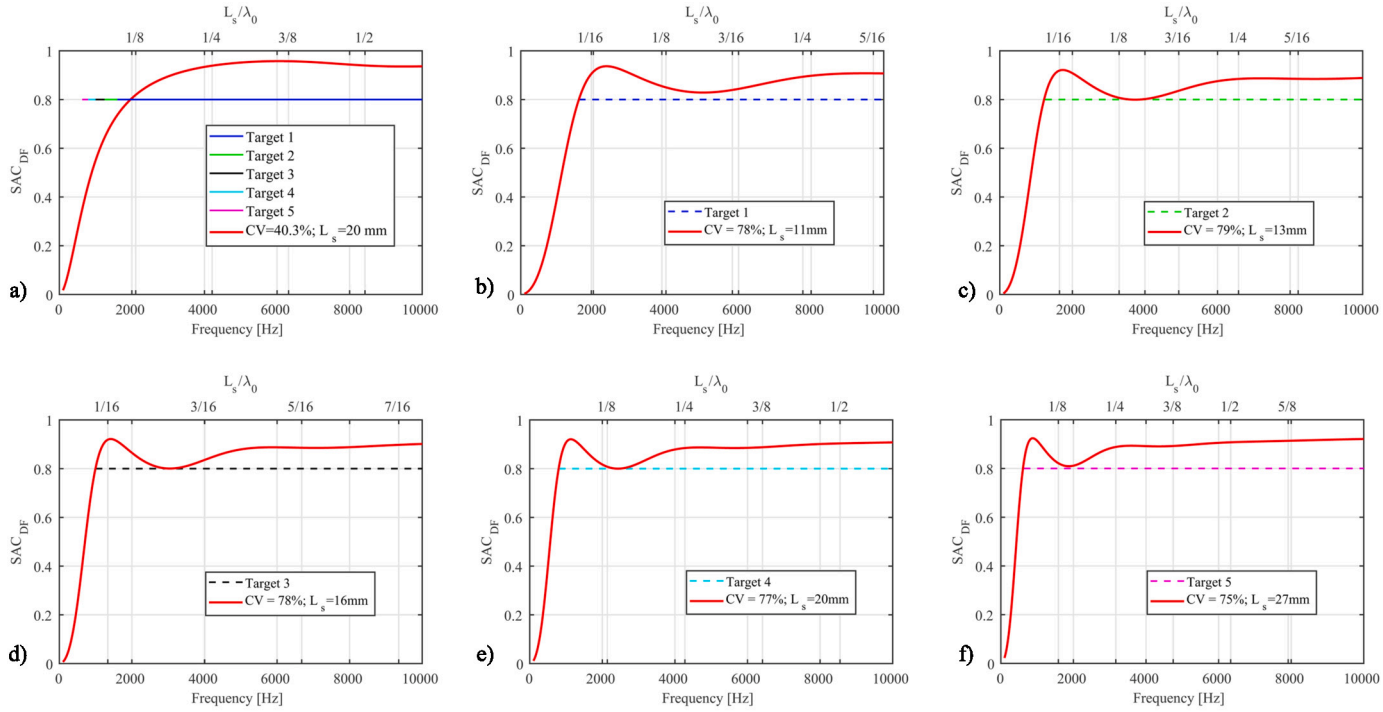

Fig. 6. Diffuse field sound absorption coefficient SAC_{DF} as a function of frequency for cotton felt F1: (a) initial configuration with $CV = 40.3\%$ and $L_s = 20mm$. The next panels (b) to (f) represent the optimized configurations satisfying targets of increasing difficulty when the polydispersity degree (CV) is allowed to be increased as a microstructural optimization lever, for the targets listed in the legend.

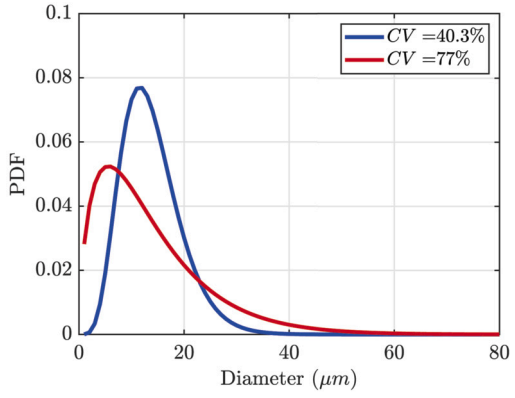

Fig. 7. Comparison of the Gamma distribution of fiber diameters obtained through SEM images ($CV = 40.3\%$), cotton felt F1 and the Gamma distribution of fiber diameters required to reach Target 4 ($CV = 77\%$).

Table 2
Fiber families with a moderate polydispersity degree ($CV \approx 15\%$) and the corresponding ratios determined in order to reconstruct distribution of fiber diameters corresponding to classes of fibrous media with increasing sound absorption and polydispersity degree ($CV \approx 30\%$, Class 3; $CV \approx 60\%$, Class 2; $CV \approx 75\%$, Class 1) at constant mean fiber diameter D_m and layer thickness ($L_s = 20\ mm$).

Fiber	Dimensionless diameter (D_i/D_m)	Class 3	Class 2	Class 1
1	0.28	-	-	28%
2	0.34	-	20%	-
3	0.64	-	25%	24%
4	0.72	24%	-	-
5	0.91	43%	18%	10%
6	1.30	33%	24%	21%
7	1.35	-	-	-
8	1.41	-	-	-
9	1.69	-	-	-
10	1.98	-	14%	15%
11	4.30	-	-	3%

Here, we show that combining several fiber families with moderate polydispersity degree ($CV \approx 15\%$) and appropriate ratios (Table 2) can exhibit reconstructed fiber distributions of increasing polydispersity degree ($CV = 30\%$, $CV = 60\%$, $CV = 75\%$) with an improved level of sound absorption (Class 3, Class 2, Class 1); Fig. 8. While the reconstructed fiber distributions may not perfectly match the targeted ones due to a limited number of existing fiber families, the associated discrepancies in sound absorption coefficients are minor. This reconstruction method offers a promising solution for achieving a highly polydisperse fiber distribution with controlled characteristics.

Another promising and complementary approach for achieving a controlled fiber diameter distribution with a high degree of polydispersity is to consider emerging techniques for the fabrication of nanofibers [32,33]. In our forthcoming work, we aim to leverage nanofiber fabrication techniques on a chosen basis of polydisperse fiber diameters in our experiments to achieve improved 3D-RF structures with controlled distribution of fiber diameters.

4. Summary

In summary, this article highlights the potential of using three-dimensional random fibrous microstructures with various distributions of fiber diameters as a way to control visco-thermal dissipation mechanisms in sound absorbing materials. This approach offers numerous advantages including tuning transport parameters across a broad range of values, enhancing the sound absorption average and achieving targets of sound absorption in diffuse field with increasing levels of difficulty. However, challenges persist, such as manufacturing a wide distribution of fiber diameters with prescribed properties. To overcome this challenge, we suggest reconstructing the prescribed distribution with a limited set of six or more families of fibers carefully selected, and exploring the synthesis of nanofibers through emerging techniques such as the electro-spinning method. These perspectives offer promising avenues for further advancements in the field of utilizing 3D-RF microstructures for advanced sound absorbing materials.

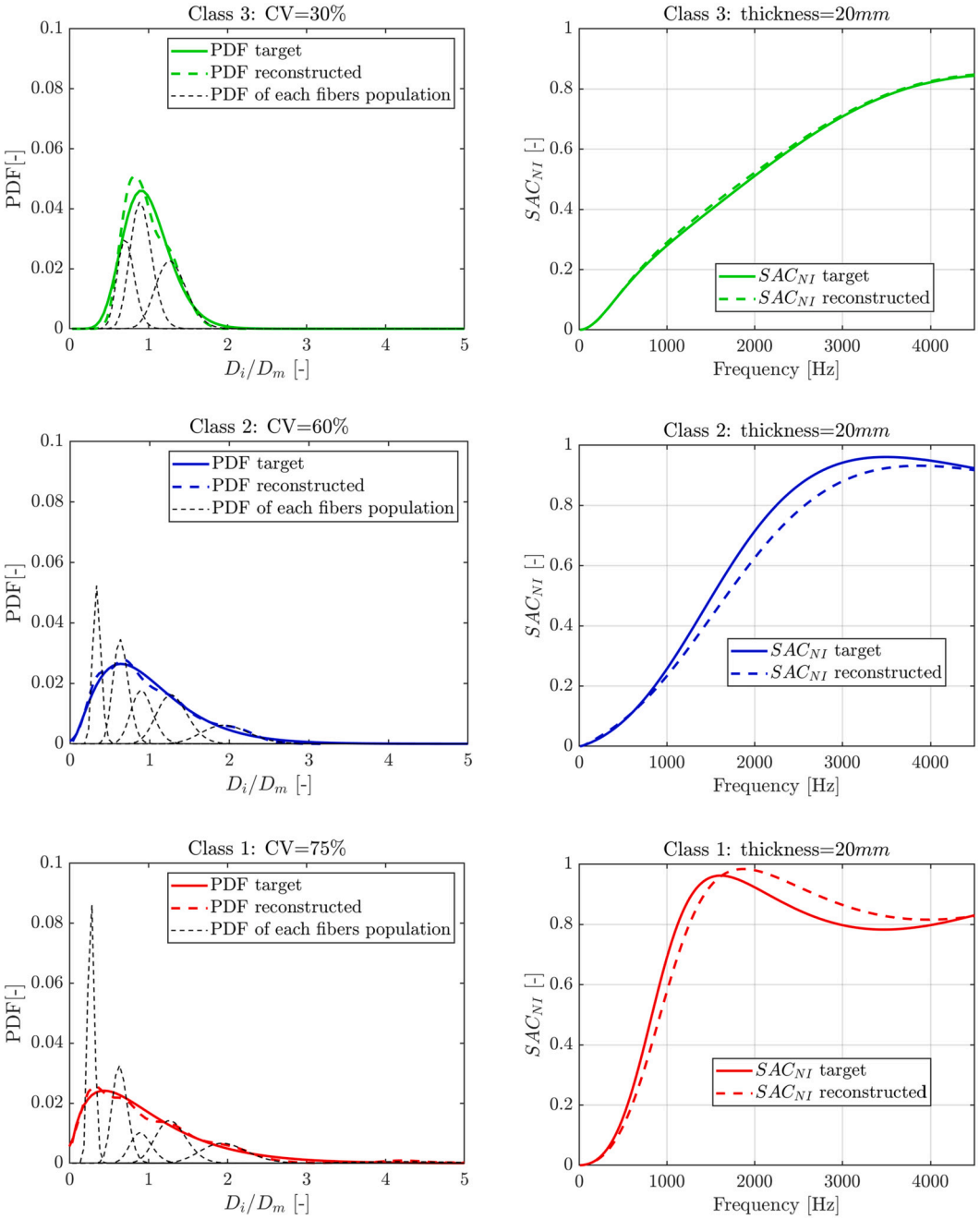

Fig. 8. Gamma distribution of fiber diameters at constant mean fiber diameter D_m for an increasing polydispersity degree ($CV = 30\%$,$CV = 60\%$, $CV = 75\%$); left panel. The dotted lines represent the distributions of each fibers population taken from an existing database (Table 2) from which a targeted degree of polydispersity (solid line) can be approximately reconstructed (dashed line). The sound absorbing coefficient at normal incidence (SAC_{NI}) as a function of frequency for each distribution of fiber diameters is plotted for a sample thickness L_s of 20 mm in the two cases listed in the legend; right panel.

Table A.3
Key parameters of the differential evolution (DE) algorithm used in the optimization studies.

	Section 2.3.2	Section 2.3.3
Fixed parameters	L_s, ϕ, D_m, β	ϕ, D_m, β, f_t
Optimized parameters	CV	L_s, CV
Constraints	$10\% \leq CV \leq 300\%$	$1\ mm \leq L_s \leq 100\ mm$ $10\% \leq CV \leq 300\%$
Fitness function (cost function)	Minimize: $1 - SAA_{NI}^{125-4500}$ $SAA_{NI}^{125-4500}$ given in Eq. (2)	Minimize: $1 - SAC_{DF}$ with $SAC_{DF} \geq 0.8$ for $f_i \geq f_t$ SAC_{DF} given in Eq. (9)
Population size	10	10
Maximum number of generations	100	100
Mutation control parameter	0.5	0.5
Crossover control parameter	0.9	0.9
Mutation strategy	DE/rand/1	DE/rand/1

CRediT authorship contribution statement

Quang Vu Tran: Writing – review & editing, Writing – original draft, Visualization, Validation, Supervision, Software, Methodology, Investigation, Formal analysis, Data curation, Conceptualization. **Camille Perrot:** Writing – review & editing, Writing – original draft, Visualization, Validation, Supervision, Software, Resources, Project administration, Methodology, Investigation, Funding acquisition, Formal analysis, Data curation, Conceptualization. **Raymond Panneton:** Writing – review & editing, Writing – original draft, Visualization, Validation, Supervision, Software, Resources, Project administration, Methodology, Investigation, Funding acquisition, Formal analysis, Data curation, Conceptualization. **Minh Tan Hoang:** Writing – review & editing, Validation, Supervision, Software, Resources, Project administration, Methodology, Investigation, Formal analysis, Conceptualization. **Ludovic Dejaeger:** Writing – review & editing, Validation, Supervision, Resources, Methodology, Investigation, Funding acquisition, Formal analysis, Conceptualization. **Valérie Marcel:** Writing – review & editing, Validation, Supervision, Resources, Project administration, Methodology, Investigation, Funding acquisition, Formal analysis, Conceptualization. **Mathieu Jouve:** Writing – review & editing, Validation, Resources, Methodology, Investigation.

Declaration of competing interest

The authors declare the following financial interests/personal relationships which may be considered as potential competing interests: Quang Vu Tran reports financial support, administrative support, and article publishing charges were provided by Gustave Eiffel University (Ref. EIFFEL 2021-00120). Quang Vu Tran reports financial support and administrative support were provided by Natural Sciences and Engineering Research Council of Canada. Quang Vu Tran reports financial support was provided by Association Nationale de la Recherche et de la Technologie. If there are other authors, they declare that they have no known competing financial interests or personal relationships that could have appeared to influence the work reported in this paper.

Acknowledgements

This work was supported by the Association Nationale de la Recherche et de la Technologie and Adler Pelzer Group under convention Cifre No. 2020/0122 (Ref. EIFFEL 2021-00120) and the Natural Sciences and Engineering Research Council of Canada (Ref. RGPIN-2018-06113). We greatly acknowledge the fruitful discussions with Jean-Yves Curien during the course of this work.

Appendix A. Key parameters of the differential evolution (DE) algorithm used in the optimization studies

The optimizations in Sec. 2.3.2 and Sec. 2.3.3 used a differential evolution (DE) algorithm [34,35]. This evolutionary algorithm works by iteratively improving a population of potential solutions over multiple generations. Each solution is represented by a set of parameters. The algorithm uses mutation to create variations, crossover to combine features, and selection to choose the best individuals based on their performance in minimizing a fitness function. Based on Sec. 2.3.2 and Sec. 2.3.3, Table A.3 summarizes the key parameters used for both optimizations.

Data availability

Data will be made available on request.

References

[1] G. Bhat, S. Malkan, Polymer-laid web formation, in: S. Russell (Ed.), Handbook of Nonwovens, in: Woodhead Publishing Series in Textiles, Woodhead Publishing, 2007, pp. 143–200.
[2] S. Gramsch, A. Klar, G. Leugering, N. Marheineke, C. Nessler, C. Strohmeyer, R. Wegener, Aerodynamic web forming: process simulation and material properties, J. Math. Ind. 6 (2016) 1–23, https://doi.org/10.1186/s13362-016-0034-4.
[3] A. Ahmed, Nonwoven fabric finishing, in: S. Russell (Ed.), Handbook of Nonwovens, in: Woodhead Publishing Series in Textiles, Woodhead Publishing, 2007, pp. 368–400.
[4] W. Albrecht, H. Fuchs, W. Kittelmann, Nonwoven Fabrics: Raw Materials, Manufacture, Applications, Characteristics, Testing Processes, John Wiley & Sons, 2006.
[5] L. Lei, N. Dauchez, J. Chazot, Prediction of the six parameters of an equivalent fluid model for thermocompressed glass wools and melamine foam, Appl. Acoust. 139 (2018) 44–56, https://doi.org/10.1016/j.apacoust.2018.04.010.
[6] X. Tang, X. Yan, Acoustic energy absorption properties of fibrous materials: a review, Composites, Part A, Appl. Sci. Manuf. 101 (2017) 360–380, https://doi.org/10.1016/j.compositesa.2017.07.002, https://www.sciencedirect.com/science/article/pii/S1359835X17302609.
[7] J. Ning, Y. Li, Dynamic flow resistivity and sound absorption of compressed fibrous porous materials: experimental and theoretical, Phys. Fluids 32 (2020) 127103, https://doi.org/10.1063/5.0029879.
[8] J. Auriault, Dynamic behaviour of a porous medium saturated by a newtonian fluid, Int. J. Eng. Sci. 18 (1980) 775–785.
[9] R. Burridge, J.B. Keller, Poroelasticity equations derived from microstructure, J. Acoust. Soc. Am. 70 (1981) 1140–1146.
[10] V. Tarnow, Airflow resistivity of models of fibrous acoustic materials, J. Acoust. Soc. Am. 100 (1996) 3706–3713, https://doi.org/10.1121/1.417233.
[11] O. Umnova, K. Attenborough, K.M. Li, Cell model calculations of dynamic drag parameters in packings of spheres, J. Acoust. Soc. Am. 107 (2000) 3113–3119, https://doi.org/10.1121/1.429340.
[12] B.P. Semeniuk, E. Lundberg, P. Göransson, Acoustics modelling of open-cell foam materials from microstructure and constitutive properties, J. Acoust. Soc. Am. 149 (2021) 2016–2026, https://doi.org/10.1121/10.0003824.
[13] G. Núñez, R. Venegas, T.G. Zieliński, F.-X. Bécot, Equivalent fluid approach to modeling the acoustical properties of polydisperse heterogeneous porous composites, Phys. Fluids 33 (2021) 062008, https://doi.org/10.1063/5.0054009.
[14] D. Johnson, J. Koplik, R. Dashen, Theory of dynamic permeability and tortuosity in fluid-saturated porous media, J. Fluid Mech. 176 (1987) 379–402, https://doi.org/10.1017/s0022112087000727.
[15] D. Lafarge, P. Lemarinier, J.-F. Allard, V. Tarnow, Dynamic compressibility of air in porous structures at audible frequencies, J. Acoust. Soc. Am. 102 (1997) 1995–2006, https://doi.org/10.1121/1.419690.
[16] V. Langlois, High-frequency permeability of porous media with thin constrictions. I. Wedge-shaped porous media, Phys. Fluids 34 (2022) 077119, https://doi.org/10.1063/5.0086257.

[17] V. Langlois, C.T. Nguyen, C. Perrot, High-frequency permeability of porous media with thin constrictions. II. Porous media containing thin holed membranes, Phys. Fluids 34 (2022) 077120, https://doi.org/10.1063/5.0093672.
[18] A.M. Chapman, J.J.L. Higdon, Oscillatory Stokes flow in periodic porous media, Phys. Fluids A, Fluid Dyn. 4 (1992) 2099–2116, https://doi.org/10.1063/1.858507.
[19] N. Martys, E. Garboczi, Length scales relating the fluid permeability and electrical conductivity in random two-dimensional model porous media, Phys. Rev. D 46 (1992) 6080, https://doi.org/10.1103/physrevb.46.6080.
[20] A. Koponen, D. Kandhai, E. Hellen, M. Alava, A. Hoekstra, M. Kataja, K. Niskanen, P. Sloot, J. Timonen, Permeability of three-dimensional random fiber webs, Phys. Rev. Lett. 80 (1998) 716, https://doi.org/10.1103/physrevlett.80.716.
[21] C. Peyrega, D. Jeulin, Estimation of acoustic properties and of the representative volume element of random fibrous media, J. Appl. Phys. 113 (2013) 104901, https://doi.org/10.1063/1.4794501.
[22] Q.V. Tran, C. Perrot, R. Panneton, M.T. Hoang, L. Dejaeger, V. Marcel, M. Jouve, Effect of polydispersity on the transport and sound absorbing properties of three-dimensional random fibrous structures, Int. J. Solids Struct. 296 (2024) 112840, https://doi.org/10.1016/j.ijsolstr.2024.112840, https://www.sciencedirect.com/science/article/pii/S0020768324001999.
[23] V. Trinh, J. Guilleminot, C. Perrot, On the sensitivity of the design of composite sound absorbing structures, Mater. Des. 210 (2021) 110058.
[24] A. Mousavi, M. Berggren, E. Wadbro, Extending material distribution topology optimization to boundary-effect-dominated problems with applications in viscothermal acoustics, Mater. Des. 234 (2023) 112302.
[25] Z. Guo, Z. Li, K. Zeng, X. Lu, J. Ye, Z. Wang, Hierarchical-porous acoustic metamaterials: a synergic approach to enhance broadband sound absorption, Mater. Des. 241 (2024) 112943.
[26] D.L. Johnson, J. Koplik, L.M. Schwartz, New pore-size parameter characterizing transport in porous media, Phys. Rev. Lett. 57 (1986) 2564, https://doi.org/10.1103/physrevlett.57.2564.
[27] M. He, C. Perrot, J. Guilleminot, P. Leroy, G. Jacqus, Multiscale prediction of acoustic properties for glass wools: computational study and experimental validation, J. Acoust. Soc. Am. 143 (2018) 3283–3299, https://doi.org/10.1121/1.5040479.
[28] S.G. Advani, C.L. Tucker III, The use of tensors to describe and predict fiber orientation in short fiber composites, J. Rheol. 31 (1987) 751–784, https://doi.org/10.1122/1.549945.
[29] H.T. Luu, C. Perrot, R. Panneton, Influence of porosity, fiber radius and fiber orientation on the transport and acoustic properties of random fiber structures, Acta Acust. Acust. 103 (2017) 1050–1063.
[30] Y. Champoux, J.-F. Allard, Dynamic tortuosity and bulk modulus in air-saturated porous media, J. Appl. Phys. 70 (1991) 1975–1979, https://doi.org/10.1063/1.349482.
[31] J.-P. Groby, N. Jiménez, V. Romero-García, Acoustic Metamaterial Absorbers, Springer, Cham, 2021, pp. 167–204.
[32] G. Chang, X. Zhu, A. Li, W. Kan, R. Warren, R. Zhao, X. Wang, G. Xue, J. Shen, L. Lin, Formation and self-assembly of 3d nanofibrous networks based on oppositely charged jets, Mater. Des. 97 (2016) 126–130.
[33] I. Alghoraibi, S. Alomari, Different Methods for Nanofiber Design and Fabrication, Springer International Publishing, 2019, pp. 79–124.
[34] R. Storn, K. Price, Differential evolution - a simple and efficient heuristic for global optimization over continuous spaces, J. Glob. Optim. 11 (1997) 341–359, https://doi.org/10.1023/A:1008202821328.
[35] K. Price, R. Storn, J. Lampinen, Differential Evolution-A Practical Approach to Global Optimization, vol. 141, 2005.